

# Mathematical, Thermodynamical, and Experimental Necessity for Coarse Graining Empirical Densities and Currents in Continuous Space

Cai Dieball and Aljaž Godec\*

Mathematical bioPhysics Group, Max Planck Institute for Multidisciplinary Sciences, Am Faßberg 11, 37077 Göttingen

We present general results on fluctuations and spatial correlations of the coarse-grained empirical density and current of Markovian diffusion in equilibrium or non-equilibrium steady states on all time scales. We unravel a deep connection between current fluctuations and generalized time-reversal symmetry, providing new insight into time-averaged observables. We highlight the essential role of coarse graining in space from mathematical, thermodynamical, and experimental points of view. Spatial coarse graining is required to uncover salient features of currents that break detailed balance, and a thermodynamically "optimal" coarse graining ensures the most precise inference of dissipation. Defined without coarse graining, the fluctuations of empirical density and current are proven to diverge on all time scales in dimensions higher than one, which has far-reaching consequences for the central-limit regime in continuous space. We apply the results to examples of irreversible diffusion. Our findings provide new intuition about time-averaged observables and allow for a more efficient analysis of single-molecule experiments.

Single-molecule experiments [1–5] probe equilibrium and non-equilibrium (i.e. detailed balance violating) processes during relaxation [6–12] or in steady states [13–21] on the level of individual trajectories. These are typically analyzed by averaging along individual realizations yielding random quantities with nontrivial statistics [22, 23]. Time-averaged observables, in particular generalized currents, are central to stochastic thermodynamics [16, 24–28]. Such time-average statistical mechanics focuses on functionals of a trajectory  $(\mathbf{x}_\tau)_{0 \leq \tau \leq t}$ , in particular the empirical density (or occupation time [29–37])  $\bar{\rho}_\mathbf{x}(t)$  and current  $\bar{\mathbf{J}}_\mathbf{x}(t)$  at a point  $\mathbf{x}$ . Necessary in the analysis of laboratory [1, 38] or computer [39] experiments with a finite spatial resolution, and useful for smoothing data *a posteriori* to improve statistics, the density and current should be defined as spatial averages over a window  $U_\mathbf{x}^h(\mathbf{x}')$  at  $\mathbf{x}$  with coarse-graining scale  $h$

$$\begin{aligned}\bar{\rho}_\mathbf{x}^U(t) &\equiv \frac{1}{t} \int_0^t U_\mathbf{x}^h(\mathbf{x}_\tau) d\tau \\ \bar{\mathbf{J}}_\mathbf{x}^U(t) &\equiv \frac{1}{t} \int_{\tau=0}^{\tau=t} U_\mathbf{x}^h(\mathbf{x}_\tau) \circ d\mathbf{x}_\tau,\end{aligned}\quad (1)$$

where  $\circ d\mathbf{x}_\tau$  denotes the Stratonovich integral. These observables are illustrated in terms of sojourns of the window in Fig. 1a,b. Choosing the window  $U_\mathbf{x}^h$  as a bin, the density and current observables appear as histograms along single trajectories over occupations of or displacements in the bin that fluctuate between different realizations (see Fig. 1c-e and accompanying extended paper [40]). Aside from coarse graining, the integration over  $U_\mathbf{x}^h(\mathbf{x}')$  may also represent a pathwise thermodynamic potential, e.g. heat dissipation (the force integrated along a stochastic path  $\int_{\tau=0}^{\tau=t} \mathbf{F}(\mathbf{x}_\tau) \cdot \circ d\mathbf{x}_\tau$  [24]) or generalized currents [18, 27, 28, 41]. Normalized windows, i.e.  $\int U_\mathbf{x}^h(\mathbf{z}) d\mathbf{z} = 1$ , yield  $\bar{\rho}_\mathbf{x}^U(t)$  and  $\bar{\mathbf{J}}_\mathbf{x}^U(t)$  that are

estimators of the probability density and current density, respectively. The usually defined empirical density,  $\bar{\rho}_\mathbf{x}(t)$ , and current,  $\bar{\mathbf{J}}_\mathbf{x}(t)$ , [14, 42–50] correspond to no coarse graining, i.e.  $U_\mathbf{x}^{h=0}(\mathbf{z})$  being Dirac's delta function  $\delta(\mathbf{x} - \mathbf{z})$ .

*Reliably* inferring from noisy trajectories whether a system obeys detailed balance, notwithstanding recent progress [1, 2, 38, 39, 51–55], remains challenging. *Quantifying* violations of detailed balance is a daunting task. One can quantify broken detailed balance through violations of the fluctuation dissipation theorem [19, 56, 57], which requires perturbing the system from the steady state. One can also check for a symmetry breaking of forward/backward transition-path times [53, 54], measure the entropy production [51, 55, 58, 59], or infer steady-state currents (see arrows in Fig. 1c) directly [1, 38], all of which require substantial statistics. However, single-molecule experiments often cannot reach ergodic times, have a finite resolution, and only allow for a limited number of repetitions. This leads to uncertainties in estimates of observables such as steady-state currents (see Fig. 1d-f). Notably, fluctuations of  $\bar{\rho}_\mathbf{x}^U$  and  $\bar{\mathbf{J}}_\mathbf{x}^U$  encode information about violations of detailed balance (even where the mean current or its components locally vanish; see Fig. 1d,e), which *a priori* is hard to interpret.

Current fluctuations have a noise floor—they are bounded from below by the “thermodynamic uncertainty relation” [16–18] which in turn allows for bounding dissipation in a system from below by current fluctuations [26, 60–62]. As we show in Fig. 1f (see [40] for a multi-well potential) the precision of inferring dissipation typically depends non-monotonically on the coarse-graining scale  $h$ —given a system, a point  $\mathbf{x}$ , and trajectory length  $t$  there exists a thermodynamically “optimal” coarse graining due to a diverging variance for  $h \rightarrow 0$  and vanishing mean for large  $h$ . Moreover,  $\bar{\rho}_\mathbf{x}$  and  $\bar{\mathbf{J}}_\mathbf{x}$  without coarse graining turn out to be ill-defined.

In systems and on time scales where dynamics is rea-

\* agodec@mpinat.mpg.de

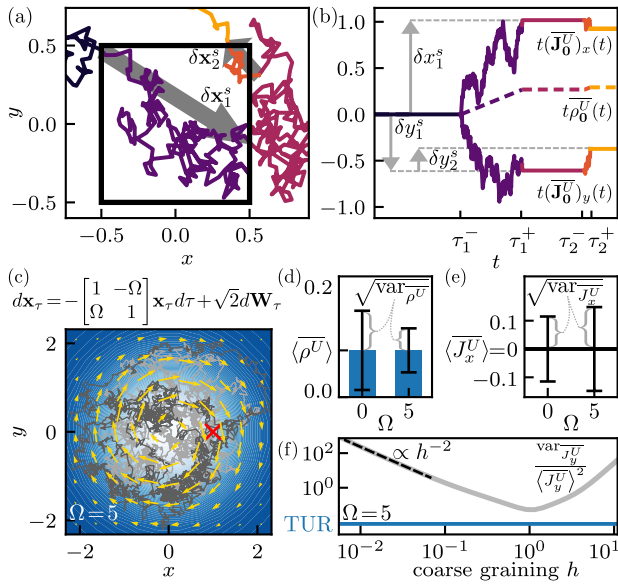


FIG. 1. (a) Diffusive trajectory traversing an observation window  $U_0^h(x, y) = 1$  if  $|x|, |y| \leq 1/2$  and  $U_0^h(x, y) = 0$  otherwise, with time running from dark to bright. Arrows denote contributions  $\delta \mathbf{x}_i^s = (\delta x_i^s, \delta y_i^s)$  of the two sojourns in  $U_0^h$  between times  $\tau_i^-$  and  $\tau_i^+$  (see Eq. (7) in Appendix I). (b) Corresponding  $t\rho_0^U(t)$  and components of  $t\mathbf{J}_0^U(t)$  from Eq. (1) as functions of  $t$ . (c) Two trajectories ( $\mathbf{x}_\tau$ ) (gray lines) of length  $t = 5$  in confined rotational flow with  $\Omega = 5$  (arrows depict the steady-state current  $\mathbf{j}_s$ ). The red cross is the reference point  $\mathbf{x}_R = (1, 0)$  considered in (d-f). Coarse-grained density (d) and  $x$ -current (e) for a Gaussian window  $U_{\mathbf{x}_R}^h$  with  $h = 0.3$ . Fluctuations of  $\rho_{\mathbf{x}}^U$  and  $\mathbf{J}_{\mathbf{x},y}^U \equiv (\mathbf{J}_{\mathbf{x}_R}^U)_{x,y}$  encode violations of detailed balance even where  $\mathbf{J}_{\mathbf{x}}^U$  vanishes. (f) Squared relative error of  $\mathbf{J}_{\mathbf{x}}^U$  for  $U_{\mathbf{x}_R}^h$  as a function of  $h$  (gray) bounded by the thermodynamic uncertainty relation (TUR; blue). A variance diverging as  $h^{-2}$  (dashed) as  $h \rightarrow 0$  and vanishing mean for  $h \gg 1$  allow for intermediate  $h$  optimizing the TUR-bound and thus the inferred dissipation.

sonably described by a Markov jump process on a small state space, current fluctuations are well understood [15, 16, 46, 63–77]. However, dynamics typically evolves in continuous space, and a continuous dynamics observed on a discrete space is *not* Markovian [78, 79] (see [80] for a quantitative confirmation). An accurate Markov jump description may require too many states to be practical, and is known to fail when considering functionals as in Eq. (1) [79]. We therefore focus on continuous space, where, with exceptions [14, 18, 81, 82], insight is limited to hydrodynamic scales [66, 68, 83] and large deviations [42–50]. A comprehensive understanding of fluctuations and spatial correlations of density and current in continuous space remains elusive, and the interpretation of the typical definition without coarse graining in dimensions  $d \geq 2$  apparently requires a revision, see below.

Here, we provide general results on the empirical density and current in overdamped diffusive steady-state systems, revealing a mathematical, thermodynamical, and

experimental necessity for spatial coarse graining. When defined in a point, fluctuations are proven to diverge in spatial dimensions above one, contradicting existing central-limit statements. We explain why a systematic variation of the coarse-graining scale provides deeper insight about the underlying dynamics and allows for improved inference of the system’s thermodynamics. Exploiting a generalized time-reversal symmetry we provide intuition about fluctuating currents along individual trajectories. Non-vanishing density-current correlations are shown to unravel violations of detailed balance from short measurements. Our results allow for a more consistent and efficient analysis of experiments, and provide new insight into non-equilibrium steady states and their thermodynamics.

*Setup.*—We consider time-homogeneous overdamped Langevin dynamics [84, 85] in  $d$ -dimensional space evolving according to the stochastic differential equation  $d\mathbf{x}_\tau = \mathbf{F}(\mathbf{x}_\tau)d\tau + \boldsymbol{\sigma}d\mathbf{W}_\tau$ , where  $d\mathbf{W}_\tau$  is the increment of a  $d$ -dimensional Wiener processes (i.e. white noise) with covariance  $\langle dW_{\tau,i}dW_{\tau',j} \rangle = \delta(\tau - \tau')\delta_{ij}d\tau d\tau'$ . The Fokker-Planck equation for the conditional probability density with initial condition  $G(\mathbf{x}, 0|\mathbf{y}) = \delta(\mathbf{x} - \mathbf{y})$  reads  $(\partial_t + \nabla_{\mathbf{x}} \cdot \hat{\mathbf{j}}_{\mathbf{x}})G(\mathbf{x}, t|\mathbf{y}) = 0$  with current operator  $\hat{\mathbf{j}}_{\mathbf{x}} \equiv \mathbf{F}(\mathbf{x}) - \mathbf{D}\nabla_{\mathbf{x}}$ , where  $\mathbf{D} \equiv \boldsymbol{\sigma}\boldsymbol{\sigma}^T/2$  is the positive definite diffusion matrix. All results directly generalize to multiplicative noise (see [40]). The drift  $\mathbf{F}(\mathbf{x})$  is assumed to be sufficiently smooth and confining to ensure the existence of a steady-state density  $G(\mathbf{x}, t \rightarrow \infty|\mathbf{y}) = p_s(\mathbf{x})$  and, if detailed balance is violated, a steady-state current  $\mathbf{j}_s(\mathbf{x}) \equiv \hat{\mathbf{j}}_{\mathbf{x}}p_s(\mathbf{x}) \neq \mathbf{0}$  [84, 85].

*Correlations and fluctuations from paths.*—To investigate the non-trivial statistics of the observables in Eq. (1) we now outline the derivation detailed in [40] of results for mean values, correlations and fluctuations assuming steady-state initial conditions. Let  $\langle \cdot \rangle_s$  denote the average over all paths  $\{\mathbf{x}_\tau\}$  evolving from  $p_s$ . The mean values  $\langle \rho_{\mathbf{x}}^U(t) \rangle_s = \int d\mathbf{z}U_{\mathbf{x}}^h(\mathbf{z})p_s(\mathbf{z})$  and  $\langle \mathbf{J}_{\mathbf{x}}^U(t) \rangle_s = \int d\mathbf{z}U_{\mathbf{x}}^h(\mathbf{z})\mathbf{j}_s(\mathbf{z})$  [40] are time-independent estimators of the steady-state density and current coarse-grained over a window  $U_{\mathbf{x}}^h$ . In contrast to the mean values, covariances display a non-trivial time-dependence and therefore contain salient features of the dynamics. We define the two-point steady-state covariance as

$$C_{AB}^{\mathbf{x}\mathbf{y}}(t) \equiv \langle A_{\mathbf{x}}(t)B_{\mathbf{y}}(t) \rangle_s - \langle A_{\mathbf{x}}(t) \rangle_s \langle B_{\mathbf{y}}(t) \rangle_s, \quad (2)$$

where  $A$  and  $B$  are either  $\rho^U$  or  $\mathbf{J}^U$ , respectively. We refer to the case  $A \neq B$  or  $\mathbf{x} \neq \mathbf{y}$  as (linear) correlations and to  $A = B$  with  $\mathbf{x} = \mathbf{y}$  as fluctuations with the notation  $\text{var}_A^{\mathbf{x}}(t) \equiv C_{AA}^{\mathbf{x}\mathbf{x}}(t)$ . Recall that  $\text{var}_\rho^{\mathbf{x}}(t)$  and  $\text{var}_{\mathbf{j}}^{\mathbf{x}}(t)$  quantify (experimentally relevant) fluctuations of histograms along single trajectories (see Fig. 1d,e), and  $\text{var}_{\mathbf{j}}^{\mathbf{x}}(t)$  is at the heart of the thermodynamic uncertainty relation (see Fig. 1f). Moreover,  $C_{\mathbf{j}\rho}^{\mathbf{x}\mathbf{y}}(t)$  was recently found to play a vital role in stochastic thermodynamics [28]. All  $C_{AB}^{\mathbf{x}\mathbf{y}}(t)$  are easily inferred from data, but lack physical understanding. We now give  $C_{AB}^{\mathbf{x}\mathbf{y}}(t)$

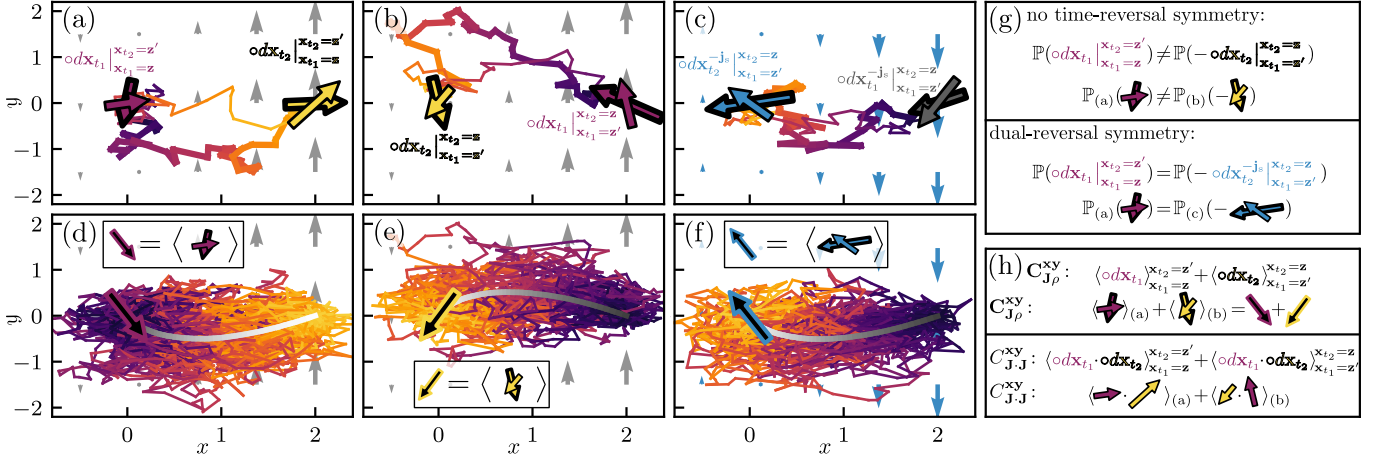


FIG. 2. (a) Two sample trajectories in a shear flow  $\mathbf{F}_{\text{sh}}(\mathbf{x})$  (grey arrows) with Stratonovich displacements  $\circ d\mathbf{x}_t$  in the initial  $\mathbf{x}_{t_1} = \mathbf{z}$  and final point  $\mathbf{x}_{t_2} = \mathbf{z}'$  for fixed  $t_1 < t_2$  depicted by purple and yellow arrows, respectively. Time is running from dark to bright. (b) Trajectories as in (a) but running from  $\mathbf{x}_{t_1} = \mathbf{z}'$  to  $\mathbf{x}_{t_2} = \mathbf{z}$ . (c) As in (b) but with the inverted shear flow  $-\mathbf{F}_{\text{sh}}(\mathbf{x}')$  (blue background arrows) and initial and final increments depicted by grey and blue arrows. (d) Ensemble of paths from  $\mathbf{x}_{t_1} = \mathbf{z}$  to  $\mathbf{x}_{t_2} = \mathbf{z}'$  contributing to  $P_{\mathbf{z}}(\mathbf{z}', t_2 - t_1)$ . The average initial displacement  $\langle \circ d\mathbf{x}_t \rangle_{\mathbf{x}_{t_1}=\mathbf{z}}^{\mathbf{x}_{t_2}=\mathbf{z}'}$  is depicted by the black-purple arrow, and the mean path  $\mathbf{z} \rightarrow \mathbf{z}'$  in time  $t_2 - t_1$  by the gray gradient line. (e) As in (d) but corresponding to (b) instead of (a). (f) As in (e) but with the reversed shear flow as in (c). (g-h) Since the shear flow breaks time-reversal symmetry, initial-point increments in (a) cannot be obtained by inverting final-point increments in (b). By dual-reversal symmetry initial-point increments follow from inverting the final-point increments in the inverted shear flow in (c), which explains initial point increments  $\circ d\mathbf{x}_{t_1}$  in current-density correlations and current (co)variances via the easier and more intuitive final point increments  $\circ d\mathbf{x}_{t_2}^{-\mathbf{j}_s}$ .

a physical meaning in terms of the statistics of paths pinned at end-points  $\mathbf{z}$  and  $\mathbf{z}'$  (see Fig. 2). Introduce  $\langle \cdot \rangle_{\mathbf{x}_{t_1}=\mathbf{z}}^{\mathbf{x}_{t_2}=\mathbf{z}'} \equiv \langle \delta(\mathbf{x}_{t_1} - \mathbf{z}) \delta(\mathbf{x}_{t_2} - \mathbf{z}') \cdot \rangle_s$ , the Stratonovich increment  $\circ d\mathbf{x}_\tau \equiv \mathbf{x}_{\tau+d\tau/2} - \mathbf{x}_{\tau-d\tau/2}$ , and the operator

$$\hat{\mathcal{I}}_{\mathbf{x}\mathbf{y}}^{t,U}[\cdot] \equiv \frac{1}{t^2} \int_0^t dt_1 \int_{t_1}^t dt_2 \int d\mathbf{z} U_{\mathbf{x}}^h(\mathbf{z}) \int d\mathbf{z}' U_{\mathbf{y}}^h(\mathbf{z}')[\cdot], \quad (3)$$

where  $[\cdot]$  represents functions of  $t_1, t_2, \mathbf{z}, \mathbf{z}'$  and without loss of generality we choose the convention  $\int_{t_1}^t dt_2 \delta(t_2 - t_1) = 1/2$ . Upon plugging in mean values  $\langle A_{\mathbf{x}} \rangle_s$  and  $\langle B_{\mathbf{y}} \rangle_s$ , the definition (2) becomes [40]  $C_{\rho\rho}^{\mathbf{x}\mathbf{y}}(t) = \hat{\mathcal{I}}_{\mathbf{x}\mathbf{y}}^{t,U}[\Xi_1^{\mathbf{z}\mathbf{z}'} - 2p_s(\mathbf{z})p_s(\mathbf{z}')]$  for density-density correlations,  $C_{J\rho}^{\mathbf{x}\mathbf{y}}(t) = \hat{\mathcal{I}}_{\mathbf{x}\mathbf{y}}^{t,u}[\Xi_2^{\mathbf{z}\mathbf{z}'} - 2\mathbf{j}_s(\mathbf{z})p_s(\mathbf{z}')]$  for current-density correlations, and (see [86])  $C_{J,J}^{\mathbf{x}\mathbf{y}}(t) = \hat{\mathcal{I}}_{\mathbf{x}\mathbf{y}}^{t,U}[\Xi_3^{\mathbf{z}\mathbf{z}'} - 2\mathbf{j}_s(\mathbf{z}) \cdot \mathbf{j}_s(\mathbf{z}')]$  for current-current correlations, where we defined

$$\begin{aligned} \Xi_1^{\mathbf{z}\mathbf{z}'} &\equiv \langle 1 \rangle_{\mathbf{x}_{t_1}=\mathbf{z}}^{\mathbf{x}_{t_2}=\mathbf{z}'} + \langle 1 \rangle_{\mathbf{x}_{t_1}=\mathbf{z}'}^{\mathbf{x}_{t_2}=\mathbf{z}} \\ \Xi_2^{\mathbf{z}\mathbf{z}'} &\equiv \frac{\langle \circ d\mathbf{x}_{t_1} \rangle_{\mathbf{x}_{t_1}=\mathbf{z}}^{\mathbf{x}_{t_2}=\mathbf{z}'} + \langle \circ d\mathbf{x}_{t_2} \rangle_{\mathbf{x}_{t_1}=\mathbf{z}'}^{\mathbf{x}_{t_2}=\mathbf{z}}}{dt_1 + dt_2} \\ \Xi_3^{\mathbf{z}\mathbf{z}'} &\equiv \frac{\langle \circ d\mathbf{x}_{t_1} \cdot \circ d\mathbf{x}_{t_2} \rangle_{\mathbf{x}_{t_1}=\mathbf{z}}^{\mathbf{x}_{t_2}=\mathbf{z}'} + \langle \circ d\mathbf{x}_{t_1} \cdot \circ d\mathbf{x}_{t_2} \rangle_{\mathbf{x}_{t_1}=\mathbf{z}'}^{\mathbf{x}_{t_2}=\mathbf{z}}}{dt_1 dt_2} \end{aligned} \quad (4)$$

Eqs. (3)-(4) tie  $C_{AB}^{\mathbf{x}\mathbf{y}}$  to properties of pinned paths, weighted by  $U_{\mathbf{x}}^h(\mathbf{z}), U_{\mathbf{y}}^h(\mathbf{z}')$  and integrated over space and times  $0 \leq t_1 \leq t_2 \leq t$ . In contrast to the somewhat better understood density-density covariance [23, 29, 87],

current-density and current-current covariances involve (scalar products of) more subtle Stratonovich increments along pinned trajectories, explained graphically in Fig. 2 and further investigated in the following.

*Correlations and fluctuations from two-point densities.*—To obtain quantitative results, we evaluate the averages  $\langle \cdot \rangle_{\mathbf{x}_{t_1}=\mathbf{z}}^{\mathbf{x}_{t_2}=\mathbf{z}'}$  in terms of two-point functions  $P_{\mathbf{z}}(\mathbf{z}', t_2 - t_1) \equiv G(\mathbf{z}', t_2 - t_1 | \mathbf{z}) p_s(\mathbf{z})$ . For density-density correlations  $C_{\rho\rho}^{\mathbf{x}\mathbf{y}}$  the result is readily obtained from Eq. (4) using  $\langle 1 \rangle_{\mathbf{x}_{t_1}=\mathbf{z}}^{\mathbf{x}_{t_2}=\mathbf{z}'} = P_{\mathbf{z}}(\mathbf{z}', t_2 - t_1)$ . Conversely, Stratonovich increments, are difficult to understand and hard to evaluate, particularly *initial-point increments*  $\circ d\mathbf{x}_{t_1}$  because they are correlated with future events.

To gain intuition we examine a two-dimensional shear flow  $\mathbf{F}_{\text{sh}}(\mathbf{x}) = 2x\hat{\mathbf{y}}$  shown in Fig. 2, depicting initial-,  $\circ d\mathbf{x}_{t_1}$ , and end-point,  $\circ d\mathbf{x}_{t_2}$ , increments along forward (Fig. 2a) and time-reversed (Fig. 2b) pinned trajectories between times  $t_1 < t_2$  and their ensemble averages (Fig. 2d-e). In the accompanying extended paper [40] we show that  $\langle \circ d\mathbf{x}_{t_2} \rangle_{\mathbf{x}_{t_1}=\mathbf{z}}^{\mathbf{x}_{t_2}=\mathbf{z}'} = \hat{\mathbf{j}}_{\mathbf{z}'} P_{\mathbf{z}}(\mathbf{z}', t_2) dt_2$ , i.e. mean displacements are given by the Fokker-Planck current as expected. Moreover, when detailed balance holds, time-reversal symmetry implies  $\mathbb{P}(\circ d\mathbf{x}_{t_1} | \mathbf{x}_{t_1}=\mathbf{z})^{\mathbf{x}_{t_2}=\mathbf{z}'} = \mathbb{P}(-\circ d\mathbf{x}_{t_2} | \mathbf{x}_{t_1}=\mathbf{z}')^{\mathbf{x}_{t_2}=\mathbf{z}}$ , whereas under broken detailed balance, e.g. due to the shear flow in Fig. 2, this ceases to hold. We may, however, employ a generalized time-reversal symmetry—the *dual-reversal symmetry* (see [40] and [27, 88, 89])—

implying  $\mathbb{P}(\circ d\mathbf{x}_{t_1}^{\mathbf{x}_{t_2}=\mathbf{z}'}) = \mathbb{P}(-\circ d\mathbf{x}_{t_2}^{-\mathbf{j}_s} |_{\mathbf{x}_{t_1}=\mathbf{z}'})$  connecting ensembles with currents  $\mathbf{j}_s$  and  $-\mathbf{j}_s$  (see Fig. 2c,f,g). Via this generalized time-reversal symmetry we circumvent the correlation of  $\circ d\mathbf{x}_{t_1}$  with the future. To materialize this we isolate the irreversible drift in  $\hat{\mathbf{j}}_{\mathbf{x}} = p_s(\mathbf{x})^{-1}\mathbf{j}_s(\mathbf{x}) - p_s(\mathbf{x})\mathbf{D}\nabla_{\mathbf{x}}p_s(\mathbf{x})^{-1}$ , and introduce the dual current operator  $\hat{\mathbf{j}}_{\mathbf{x}}^{\dagger} \equiv -\hat{\mathbf{j}}_{\mathbf{x}}^{-\mathbf{j}_s} = p_s(\mathbf{x})^{-1}\mathbf{j}_s(\mathbf{x}) + p_s(\mathbf{x})\mathbf{D}\nabla_{\mathbf{x}}p_s(\mathbf{x})^{-1}$ , rendering all terms in Eq. (4) (illustrated in Fig. 2h) tractable, and ultimately leading to our main result

$$\begin{aligned} C_{\mathbf{J}\rho}^{\mathbf{xy}}(t) &= \hat{\mathcal{I}}_{\mathbf{xy}}^{t,U}[\hat{\mathbf{j}}_{\mathbf{z}}P_{\mathbf{z}'}(\mathbf{z},t') + \hat{\mathbf{j}}_{\mathbf{z}}^{\dagger}P_{\mathbf{z}'}(\mathbf{z}',t') - 2\mathbf{j}_s(\mathbf{z})p_s(\mathbf{z}')] \\ C_{\mathbf{J}\mathbf{J}}^{\mathbf{xy}}(t) &= \frac{2\text{Tr}\mathbf{D}}{t} \int d\mathbf{z}U_{\mathbf{x}}^h(\mathbf{z})U_{\mathbf{y}}^h(\mathbf{z})p_s(\mathbf{z}) + \\ &\hat{\mathcal{I}}_{\mathbf{xy}}^{t,U}[\hat{\mathbf{j}}_{\mathbf{z}} \cdot \hat{\mathbf{j}}_{\mathbf{z}'}^{\dagger}P_{\mathbf{z}'}(\mathbf{z},t') + \hat{\mathbf{j}}_{\mathbf{z}'} \cdot \hat{\mathbf{j}}_{\mathbf{z}}^{\dagger}P_{\mathbf{z}'}(\mathbf{z}',t') - 2\mathbf{j}_s(\mathbf{z}) \cdot \mathbf{j}_s(\mathbf{z}')], \end{aligned} \quad (5)$$

where the first term in  $C_{\mathbf{J}\mathbf{J}}^{\mathbf{xy}}(t)$  arises from  $t_1 = t_2$  [40], and the operator  $\hat{\mathcal{I}}_{\mathbf{xy}}^{t,U}$  simplifies  $t^{-2} \int_0^t dt_1 \int_{t_1}^t dt_2 \rightarrow t^{-1} \int_0^t dt'(1-t'/t)$  since Eq. (5) depends only on time differences  $t' \equiv t_2 - t_1 \geq 0$ . Notably, written in this simplified form Eq. (5) establishes Green-Kubo relations [90, 91] connecting covariances  $C_{AB}^{\mathbf{xy}}$  to time-integrals of generalized correlation functions.

Given the two-point function  $P_{\mathbf{z}}(\mathbf{z}',t')$ , Eq. (5) gives the correlation and fluctuations of observables defined in Eq. (1). In practice,  $P_{\mathbf{z}}(\mathbf{z}',t')$  may not necessarily be available. However, the theoretical result Eq. (5) nevertheless allows us to draw several conclusions, in particular by considering special cases and limits. At equilibrium  $\hat{\mathbf{j}}_{\mathbf{z}}^{\dagger} = -\hat{\mathbf{j}}_{\mathbf{z}}$ , implying  $C_{\mathbf{J}\rho}^{\mathbf{xy}}(t) = 0$ . A non-zero  $C_{\mathbf{J}\rho}^{\mathbf{xy}}(t)$  at any time  $t$  is thus a conclusive signature of broken detailed balance. Moreover, at equilibrium  $C_{\mathbf{J}\mathbf{J}}^{\mathbf{xy}}(t)$  does not vanish although  $\langle \overline{\mathbf{J}_{\mathbf{x}}^U} \rangle_s = 0$ . When  $\mathbf{j}_s \neq \mathbf{0}$ ,  $\text{var}_{\mathbf{J}}^{\mathbf{x}}(t) \equiv C_{\mathbf{J}\mathbf{J}}^{\mathbf{xx}}(t)$  may display maxima where  $P_s(\mathbf{x})$  has none (see Fig. 3a-c), and an oscillatory time-dependence due to circulating currents (see Fig. 3d), both signaling non-equilibrium. For a more detailed discussion of Eq. (5) see [40].

*Necessity of coarse graining.*—Of particular interest is the dependence of fluctuations on the coarse-graining length scale  $h$  (see Fig. 1f, Fig. 3c and [40]). Importantly, the limits  $h \rightarrow \infty$  and  $h \rightarrow 0$  are generally accessible from Eq. (5) independent of the detailed dynamics (see [40]). The limit  $h \rightarrow 0$  with  $U_{\mathbf{x}}^h(\mathbf{z}) \rightarrow \delta(\mathbf{x} - \mathbf{z})$  corresponds to no coarse graining, i.e. the observables Eq. (1) are evaluated in a single point  $\mathbf{z}$ . In this limit, the variance and covariance of  $\rho_{\mathbf{x}}^U$  and  $\mathbf{J}_{\mathbf{x}}^U$  for  $d \geq 2$  and any  $t$  behave as [40]

$$\begin{aligned} \text{var}_{\rho}^{\mathbf{x}}(t) &\stackrel{h \rightarrow 0}{\simeq} \frac{k p_s(\mathbf{x})}{t} \times \begin{cases} \frac{h^{2-d}}{d-2} & \text{for } d > 2 \\ -\ln h & \text{for } d = 2 \end{cases} \\ C_{\mathbf{J}\rho}^{\mathbf{xx}}(t) &\stackrel{h \rightarrow 0}{\simeq} \mathbf{j}_s(\mathbf{x}) \text{var}_{\rho}^{\mathbf{x}}(t) / 2p_s(\mathbf{x}) \\ \text{var}_{\mathbf{J}}^{\mathbf{x}}(t) &\stackrel{h \rightarrow 0}{=} \frac{k' p_s(\mathbf{x})}{t} (d-1)h^{-d} + \mathcal{O}(t^{-1})\mathcal{O}(h^{1-d}), \end{aligned} \quad (6)$$

where  $\simeq$  denotes asymptotic equality, and  $k, k'$  are constants depending on  $\mathbf{D}$  and  $U_{\mathbf{x}}$  [40]. Therefore, taking

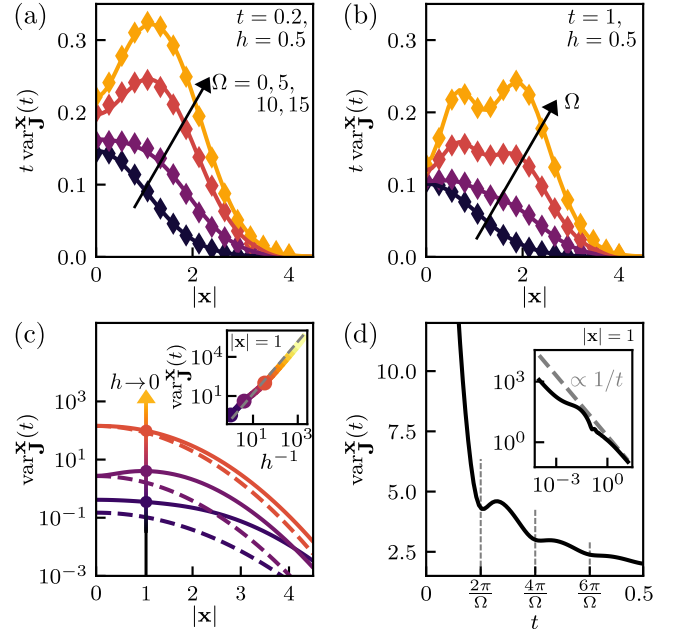


FIG. 3.  $t \text{var}_{\mathbf{J}}^{\mathbf{x}}$  as a function of the radius  $|\mathbf{x}|$  in the harmonically confined rotational flow in Fig. 1c for increasing  $\Omega$  with Gaussian  $U_{\mathbf{x}}^h$  with width  $h$  at (a)  $t = 0.2$  and (b)  $t = 1$ ; Lines depict Eq. (5) and symbols simulations [80]. (c)  $t \text{var}_{\mathbf{J}}^{\mathbf{x}}$  at  $t = 1$  for  $\Omega = 10$  (full lines) and equilibrium  $\Omega = 0$  (dashed lines), for various  $h$  decreasing along the arrow. Inset: divergence of  $\text{var}_{\mathbf{J}}^{\mathbf{x}}$  as  $h \rightarrow 0$  at  $|\mathbf{x}| = 1$ ; the dashed line depicts Eq. (6). Note the logarithmic scales. (d)  $\text{var}_{\mathbf{J}}^{\mathbf{x}}$  as a function of  $t$  for very strong driving  $\Omega = 50$ ; Inset: (d) on logarithmic scales alongside the central-limit scaling  $\propto t^{-1}$ .

$U_{\mathbf{x}}^h(\mathbf{z}) \xrightarrow{h \rightarrow 0} \delta(\mathbf{x} - \mathbf{z})$  as implicitly assumed in [23, 42–50] we find for  $d \geq 2$  that  $\text{var}_{\rho, \mathbf{J}}^{\mathbf{x}}(t), C_{\mathbf{J}\rho}^{\mathbf{xx}}(t)$  diverge for all  $t$  (see Fig. 3c). Eq. (6) also applies to Markov-jump processes defined on a grid with spacing  $h \rightarrow 0$ ; for details and an example see [80]. The divergence can be understood intuitively [40], e.g. based on the following argument.

Note that the probability that point  $\mathbf{z}$  is hit by the trajectory  $(\mathbf{x}_{\tau})_{0 \leq \tau \leq t}$ , i.e. that there is a  $\tau \in [0, t]$  such that  $\mathbf{x}_{\tau} = \mathbf{z}$ , delicately depends on the spatial dimensionality  $d$ . This probability is positive for  $d = 1$  but zero in higher-dimensional space. That is,  $\mathbb{P}(\exists \tau \in (0, t]: \mathbf{x}_{\tau} = \mathbf{z}) = 0$  for diffusion in  $d \geq 2$  [40, 92]. Mean values remain finite in the limit  $h \rightarrow 0$ , namely  $\langle \overline{\rho_{\mathbf{x}}(t)} \rangle_s = p_s(\mathbf{x})$  and  $\langle \overline{\mathbf{J}_{\mathbf{x}}(t)} \rangle_s = \mathbf{j}_s(\mathbf{x})$  in agreement with existing literature [14, 45–50, 82]. Since the probability to hit the point  $\mathbf{z}$  is approaching zero as  $h \rightarrow 0$ , this implies that the mean is precisely balanced by the infinite contribution of the delta function  $U_{\mathbf{x}}^h(\mathbf{z}) \rightarrow \delta(\mathbf{x} - \mathbf{z})$ , as in  $\langle \delta(\mathbf{x}_{\tau} - \mathbf{x}) \rangle_s = p_s(\mathbf{x})$ . Loosely speaking, here “ $0 \times \infty$ ” is finite. One may therefore expect diverging second (and higher) moments when  $h \rightarrow 0$  as this argument extends to “ $0 \times \infty^2 = \infty$ ”. The argument is not limited to overdamped motion but seems to extend to a larger class of stochastic dynamics, such as underdamped diffusion and

experimental data on anomalous intracellular transport [93] shown in Fig. 9 of Ref. [40].

We hypothesize that not only the moments diverge, but that the density and current cannot even be consistently defined for  $h = 0$ . Moreover, the limits  $h \rightarrow 0$  and  $t \rightarrow \infty$  do *not* commute. This has important consequences for the central-limit regime, i.e. statistics on longest time scales (see Appendix II and [40]). Some coarse graining  $h > 0$  is therefore necessary for mathematical consistency and anticipated central-limit properties.

Notably, for small windows Eq. (6) implies that fluctuations (unlike correlations) carry no information about steady-state currents  $\mathbf{j}_s(\mathbf{x})$  and thus violations of detailed balance and thermodynamic properties such as the system's dissipation. In this limit fluctuations reflect only Brownian, thermal currents that are invariant with respect to  $\mathbf{j}_s(\mathbf{x})$ —systems with equal  $p_s(\mathbf{x})$  and  $\mathbf{D}$  display identical fluctuations (see Eq. (6) and Fig. 3c). Recall that the dissipation can be inferred from current fluctuations via the thermodynamic uncertainty relation [16, 17, 26]. We now see that only an intermediate coarse graining, such as the “optimum” in Fig. 1f, allows to infer dissipation from fluctuations. Moreover, spatial features of steady-state currents (see Fig. 3c) are only revealed with coarse graining. Some coarse graining  $h > 0$  is thus necessary to infer thermodynamic properties. In addition, divergent fluctuations make it impossible to accurately infer densities and currents without coarse graining from experiments. Experiments also nominally have a finite spatial resolution. Thus, coarse graining is also experimentally necessary.

*Conclusion.*—Leveraging Itô calculus and generalized time-reversal symmetry we were able to provide elusive physical intuition about fluctuations and correlations of empirical densities and currents that are central to stochastic thermodynamics. We established the so far overlooked necessity for spatial coarse graining—it is required to ensure mathematically well defined observables and the validity of central-limit statements in dimensions  $d \geq 2$ , to improve the accuracy of inferring thermodynamic properties (e.g. dissipation) from fluctuations and to uncover salient features of non-equilibrium steady-state currents without inferring these individually [94–96], and is unavoidable in the analysis of experimental data with a finite resolution. Non-vanishing current-density correlations were shown to be a conclusive indicator of broken detailed balance, and may improve the accuracy of inferring invariant densities [97] and dissipation far from equilibrium [28]. Our results allow for generalizations to non-stationary initial conditions or non-ergodic dynamics, which will be addressed in forthcoming publications.

*Acknowledgments.*—Financial support from Studienstiftung des Deutschen Volkes (to C. D.) and the German Research Foundation (DFG) through the Emmy Noether Program GO 2762/1-2 (to A. G.) is gratefully acknowledged.

*Appendix I: Density and current from sojourns.*—In general the density and current functionals measure the ( $U_{\mathbf{x}}^h$ -weighted) time spent and displacement accumulated in the window  $U_{\mathbf{x}}^h$  averaged over time. Specifically, when  $U_{\mathbf{x}}^h$  is the indicator function,  $U_{\mathbf{x}}^h(\mathbf{z}) = h^{-d} \mathbb{1}_{\Omega_{\mathbf{x}}}(\mathbf{z})$ , of a region  $\Omega_{\mathbf{x}}$  centered at  $\mathbf{x}$  with volume  $h^d$ , we can write this illustratively in terms of the sojourns of the window as follows. Letting the times of entering and exiting said window be  $\tau_i^-$  and  $\tau_i^+$ , respectively,  $t\rho_{\mathbf{x}}^{\overline{U}}(t)$  corresponds to the sum of sojourn times,  $\tau_i^s = \tau_i^+ - \tau_i^-$ , and  $t\mathbf{J}_{\mathbf{x}}^{\overline{U}}(t)$  the sum of vectors  $\delta\mathbf{x}_i^s$  between entrance  $\mathbf{x}_{\tau_i^-}$  and exit  $\mathbf{x}_{\tau_i^+}$  points, that is,

$$\begin{aligned} t\rho_{\mathbf{x}}^{\overline{U}}(t) &= \frac{1}{h^d} \sum_{i \leq N_t} (\tau_i^+ - \tau_i^-) \equiv \frac{1}{h^d} \sum_{i \leq N_t} \tau_i^s \\ t\mathbf{J}_{\mathbf{x}}^{\overline{U}}(t) &= \frac{1}{h^d} \sum_{i \leq N_t} (\mathbf{x}_{\tau_i^+} - \mathbf{x}_{\tau_i^-}) \equiv \frac{1}{h^d} \sum_{i \leq N_t} \delta\mathbf{x}_i^s, \end{aligned} \quad (7)$$

where  $N_t$  is the number of visits of the window. Note that  $N_t$  is almost surely either  $\infty$  or 0, but the sum converges. The points  $\mathbf{x}_0$  or  $\mathbf{x}_t$  may lie within  $U_{\mathbf{x}}^h$  for which we set  $\mathbf{x}_{\tau_1^-} = \mathbf{x}_0$  and/or  $\mathbf{x}_{\tau_{N_t}^+} \equiv \mathbf{x}_t$ . As a result of correlations between  $\mathbf{x}_{\tau_i^-}$  and  $\tau_i^s$  as well as  $\mathbf{x}_{\tau_i^+}$  and  $\mathbf{x}_{\tau_{i+1}^-}$ ,  $t\rho_{\mathbf{x}}^{\overline{U}}$  and  $t\mathbf{J}_{\mathbf{x}}^{\overline{U}}$  are in general *not* renewal processes. A realization of  $\mathbf{x}_{\tau}$  in Fig. 1a,b provides intuition about Eq. (7).

*Appendix II: Central-limit regime.*—Since the observables defined in Eq. (1) involve time-averages, their statistics on the longest time scales is expected to be governed by the central limit theorem. Indeed, for non-zero  $h$  or in spatial dimension  $d = 1$  (in both cases we obtained finite variances) on time scales  $t$  that are very large compared to all time scales in the system, different parts of a trajectory (e.g. the sojourns in Fig. 1a and Eq. (7)) become sufficiently uncorrelated such that the central limit theorem implies Gaussian statistics. However, the diverging variance for  $h \rightarrow 0$  for  $d \geq 2$  prevents Gaussian central-limit statistics on all time scales for the empirical density and current defined with a delta-function (i.e. without coarse graining). Since the diverging part of the variance in Eq. (6) has the dominant central-limit scaling  $\propto t^{-1}$ , the asymptotic variance  $\sigma_A^2 \stackrel{t \rightarrow \infty}{\sim} t \text{var}_{\mathbf{x}}^A(t)$  (where  $A_{\mathbf{x}}(t)$  denotes  $\rho_{\mathbf{x}}^{\overline{U}}(t)$  or  $\mathbf{J}_{\mathbf{x}}^{\overline{U}}(t)$ ) also diverges as  $h \rightarrow 0$ . This implies that taking  $t \rightarrow \infty$  first and then  $h \rightarrow 0$  also does *not* yield finite variances. Moreover, note that the longest time scale in the system becomes the recurrence time, which diverges as  $h \rightarrow 0$ . We hypothesize that a limiting distribution of  $A_{\mathbf{x}}(t)$  only exists as a scaling limit where  $h \rightarrow 0$  and  $t \rightarrow \infty$  simultaneously in some  $d$ -dependent manner [40].

The central-limit regime is generally contained in the framework of large deviation theory [42, 48, 98]. Due to the divergent variance  $\sigma_A^2$  and the resulting breakdown of Gaussian central-limit statistics, any large deviation principle for empirical densities and currents without coarse graining that predicts finite variances ceases to hold in  $d \geq 2$ .

- [1] J. Gladrow, N. Fakhri, F. C. MacKintosh, C. F. Schmidt, and C. P. Broedersz, *Phys. Rev. Lett.* **116**, 248301 (2016).
- [2] F. S. Gnesotto, F. Mura, J. Gladrow, and C. P. Broedersz, *Rep. Prog. Phys.* **81**, 066601 (2018).
- [3] F. Ritort, *J. Phys.: Cond. Matt.* **18**, R531 (2006).
- [4] W. J. Greenleaf, M. T. Woodside, and S. M. Block, *Annu. Rev. Biophys. Biomol. Struct.* **36**, 171 (2007).
- [5] J. R. Moffitt, Y. R. Chemla, S. B. Smith, and C. Bustamante, *Annu. Rev. Biochem.* **77**, 205 (2008).
- [6] S. Vaikuntanathan and C. Jarzynski, *EPL (Europhys. Lett.)* **87**, 60005 (2009).
- [7] C. Maes, K. Netočný, and B. Wynants, *Phys. Rev. Lett.* **107**, 010601 (2011).
- [8] H. Qian, *J. Math. Phys.* **54**, 053302 (2013).
- [9] C. Maes, *Phys. Rev. Lett.* **119**, 160601 (2017).
- [10] N. Shiraishi and K. Saito, *Phys. Rev. Lett.* **123**, 110603 (2019).
- [11] A. Lapolla and A. Godec, *Phys. Rev. Lett.* **125**, 110602 (2020).
- [12] T. Koyuk and U. Seifert, *Phys. Rev. Lett.* **125**, 260604 (2020).
- [13] D.-Q. Jiang, M. Qian, and M.-P. Qian, *Mathematical Theory of Nonequilibrium Steady States* (Springer Berlin Heidelberg, 2004).
- [14] C. Maes, K. Netočný, and B. Wynants, *Physica A* **387**, 2675 (2008).
- [15] C. Maes and K. Netočný, *EPL (Europhys. Lett.)* **82**, 30003 (2008).
- [16] T. R. Gingrich, J. M. Horowitz, N. Perunov, and J. L. England, *Phys. Rev. Lett.* **116**, 120601 (2016).
- [17] A. C. Barato and U. Seifert, *Phys. Rev. Lett.* **114**, 158101 (2015).
- [18] A. Dechant and S.-i. Sasa, *J. Stat. Mech.*, 063209 (2018).
- [19] U. Seifert and T. Speck, *EPL (Europhys. Lett.)* **89**, 10007 (2010).
- [20] E. N. M. Cirillo, M. Colangeli, O. Richardson, and L. Rondoni, *Phys. Rev. E* **103**, 032119 (2021).
- [21] D. J. Evans, S. R. Williams, D. J. Searles, and L. Rondoni, *J. Stat. Phys.* **164**, 842 (2016).
- [22] S. Burov, J.-H. Jeon, R. Metzler, and E. Barkai, *Phys. Chem. Chem. Phys.* **13**, 1800 (2011).
- [23] A. Lapolla, D. Hartich, and A. Godec, *Phys. Rev. Research* **2**, 043084 (2020).
- [24] H. Qian, *Phys. Rev. E* **64**, 022101 (2001).
- [25] J. M. Horowitz and T. R. Gingrich, *Nat. Phys.* **16**, 15 (2019).
- [26] T. R. Gingrich, G. M. Rotskoff, and J. M. Horowitz, *J. Phys. A: Math. Theor.* **50**, 184004 (2017).
- [27] A. Dechant and S.-i. Sasa, *Phys. Rev. Research* **3**, 042012 (2021).
- [28] A. Dechant and S.-i. Sasa, *Phys. Rev. X* **11**, 041061 (2021).
- [29] M. Kac, *Trans. Am. Math. Soc.* **65**, 1 (1949).
- [30] D. A. Darling and M. Kac, *Trans. Am. Math. Soc.* **84**, 444 (1957).
- [31] E. Aghion, D. A. Kessler, and E. Barkai, *Phys. Rev. Lett.* **122**, 010601 (2019).
- [32] S. Carmi and E. Barkai, *Phys. Rev. E* **84**, 061104 (2011).
- [33] S. N. Majumdar and A. Comtet, *Phys. Rev. Lett.* **89**, 060601 (2002).
- [34] S. N. Majumdar and D. S. Dean, *Phys. Rev. E* **66**, 041102 (2002).
- [35] S. N. Majumdar, *Curr. Sci.* **89**, 2075 (2005).
- [36] A. J. Bray, S. N. Majumdar, and G. Schehr, *Adv. Phys.* **62**, 225 (2013).
- [37] G. Bel and E. Barkai, *Phys. Rev. Lett.* **94**, 240602 (2005).
- [38] C. Battle, C. P. Broedersz, N. Fakhri, V. F. Geyer, J. Howard, C. F. Schmidt, and F. C. MacKintosh, *Science* **352**, 604 (2016).
- [39] J. Li, J. M. Horowitz, T. R. Gingrich, and N. Fakhri, *Nat. Commun.* **10**, 1666 (2019).
- [40] See accompanying extended paper available at <https://arxiv.org/abs/2204.06553>.
- [41] A. Dechant, *J. Phys. A: Math. Theor.* **52**, 035001 (2018).
- [42] H. Touchette, *Phys. Rep.* **478**, 1 (2009).
- [43] S. Kusuoka, K. Kuwada, and Y. Tamura, *Probab. Theory Relat. Fields* **147**, 649 (2009).
- [44] R. Chetrite and H. Touchette, *Phys. Rev. Lett.* **111**, 120601 (2013).
- [45] R. Chetrite and H. Touchette, *Annales Henri Poincaré* **16**, 2005 (2014).
- [46] A. C. Barato and R. Chetrite, *J. Stat. Phys.* **160**, 1154 (2015).
- [47] J. Hoppenau, D. Nickelsen, and A. Engel, *New J. Phys.* **18**, 083010 (2016).
- [48] H. Touchette, *Physica A* **504**, 5 (2018).
- [49] E. Mallmin, J. du Buisson, and H. Touchette, *J. Phys. A: Math. Theor.* **54**, 295001 (2021).
- [50] C. Monthus, *J. Stat. Mech: Theory Exp.* **2021**, 063211 (2021).
- [51] É. Roldán and J. M. R. Parrondo, *Phys. Rev. Lett.* **105**, 150607 (2010).
- [52] É. Fodor, C. Nardini, M. E. Cates, J. Tailleur, P. Visco, and F. van Wijland, *Phys. Rev. Lett.* **117**, 038103 (2016).
- [53] J. Gladrow, M. Ribezzi-Crivellari, F. Ritort, and U. F. Keyser, *Nat. Commun.* **10**, 10.1038/s41467-018-07873-9 (2019).
- [54] A. M. Berezhkovskii and D. E. Makarov, *J. Phys. Chem. Lett.* **11**, 1682 (2020).
- [55] D. S. Seara, B. B. Machta, and M. P. Murrell, *Nat. Commun.* **12**, 10.1038/s41467-020-20281-2 (2021).
- [56] L. F. Cugliandolo, D. S. Dean, and J. Kurchan, *Phys. Rev. Lett.* **79**, 2168 (1997).
- [57] D. Mizuno, C. Tardin, C. F. Schmidt, and F. C. MacKintosh, *Science* **315**, 370 (2007).
- [58] U. Seifert, *Rep. Prog. Phys.* **75**, 126001 (2012).
- [59] S. Pigolotti, I. Neri, É. Roldán, and F. Jülicher, *Phys. Rev. Lett.* **119**, 140604 (2017).
- [60] U. Seifert, *Physica A* **504**, 176 (2018).
- [61] S. Otsubo, S. Ito, A. Dechant, and T. Sagawa, *Phys. Rev. E* **101**, 062106 (2020).
- [62] S. K. Manikandan, D. Gupta, and S. Krishnamurthy, *Phys. Rev. Lett.* **124**, 120603 (2020).
- [63] J. L. Lebowitz and H. Spohn, *J. Stat. Phys.* **95**, 333 (1999).
- [64] H. Qian, S. Saffarian, and E. L. Elson, *Proc. Natl. Acad. Sci. U.S.A.* **99**, 10376 (2002).
- [65] S. Pilgram, A. N. Jordan, E. V. Sukhorukov, and M. Büttiker, *Phys. Rev. Lett.* **90**, 206801 (2003).
- [66] T. Bodineau and B. Derrida, *Phys. Rev. Lett.* **92**, 180601 (2004).

- [67] D. Andrieux and P. Gaspard, *J. Stat. Phys.* **127**, 107 (2007).
- [68] L. Bertini, A. D. Sole, D. Gabrielli, G. Jona-Lasinio, and C. Landim, *Phys. Rev. Lett.* **94**, 030601 (2005).
- [69] R. K. P. Zia and B. Schmittmann, *J. Stat. Mech: Theory Exp.*, 07012 (2007).
- [70] M. Baiesi, C. Maes, and K. Netočný, *J. Stat. Phys.* **135**, 57 (2009).
- [71] P. Pietzonka, A. C. Barato, and U. Seifert, *Phys. Rev. E* **93**, 052145 (2016).
- [72] T. R. Gingrich and J. M. Horowitz, *Phys. Rev. Lett.* **119**, 170601 (2017).
- [73] S. C. Kapfer and W. Krauth, *Phys. Rev. Lett.* **119**, 240603 (2017).
- [74] K. Macieszczak, K. Brandner, and J. P. Garrahan, *Phys. Rev. Lett.* **121**, 130601 (2018).
- [75] M. Kaiser, R. L. Jack, and J. Zimmer, *J. Stat. Phys.* **170**, 1019 (2018).
- [76] A. C. Barato, R. Chetrite, A. Faggionato, and D. Gabrielli, *New J. Phys.* **20**, 103023 (2018).
- [77] S. Marcantoni, C. Pérez-Espigares, and J. P. Garrahan, *Phys. Rev. E* **101**, 062142 (2020).
- [78] D. Hartich and A. Godec, *Phys. Rev. X* **11**, 041047 (2021).
- [79] E. Suárez, R. P. Wiewiora, C. Wehmeyer, F. Noé, J. D. Chodera, and D. M. Zuckerman, *J. Chem. Theory Comput.* **17**, 3119 (2021).
- [80] See Supplemental Material at [...] for further details and auxiliary results, as well as Refs. [2–6, 99, 100].
- [81] F. Flandoli, M. Gubinelli, M. Giaquinta, and V. M. Tortorelli, *Stochastic Processes Appl.* **115**, 1583 (2005).
- [82] V. Y. Chernyak, M. Chertkov, S. V. Malinin, and R. Teodorescu, *J. Stat. Phys.* **137**, 109 (2009).
- [83] L. Bertini, A. D. Sole, D. Gabrielli, G. Jona-Lasinio, and C. Landim, *Rev. Mod. Phys.* **87**, 593 (2015).
- [84] C. W. Gardiner, *Handbook of stochastic methods for physics, chemistry, and the natural sciences* (Springer-Verlag, Berlin New York, 1985).
- [85] G. A. Pavliotis, *Stochastic Processes and Applications* (Springer New York, 2014).
- [86] Fluctuations and correlations of  $\overline{\mathbf{J}}_{\mathbf{x}}^{\mathbf{U}}(t)$  are characterized by the  $d \times d$  covariance matrix with elements  $(\mathbf{C}_{\mathbf{J}\mathbf{J}}^{\mathbf{x}\mathbf{y}}(t))_{ik} = C_{\mathbf{J}_i \mathbf{J}_k}^{\mathbf{x}\mathbf{y}}(t)$ . We focus on the scalar case  $C_{\mathbf{J}\mathbf{J}}^{\mathbf{x}\mathbf{y}}(t) \equiv \text{Tr} \mathbf{C}_{\mathbf{J}\mathbf{J}}^{\mathbf{x}\mathbf{y}}(t)$ . See [100] for the full covariance matrix.
- [87] A. Lapolla and A. Godec, *New J. Phys.* **20**, 113021 (2018).
- [88] S.-i. Sasa, *J. Stat. Mech: Theory Exp.* **2014**, P01004 (2014).
- [89] T. Hatano and S.-i. Sasa, *Phys. Rev. Lett.* **86**, 3463 (2001).
- [90] M. S. Green, *J. Chem. Phys.* **22**, 398–413 (1954).
- [91] R. Kubo, *J. Phys. Soc. Jpn.* **12**, 570–586 (1957).
- [92] R. Durrett, *Stochastic calculus: A practical introduction*, 1st ed. (CRC Press, Boca Raton, 1996).
- [93] A. Sabri, X. Xu, D. Krapf, and M. Weiss, *Phys. Rev. Lett.* **125**, 10.1103/physrevlett.125.058101 (2020).
- [94] A. Frishman and P. Ronceray, *Phys. Rev. X* **10**, 021009 (2020).
- [95] D. B. Brückner, P. Ronceray, and C. P. Broedersz, *Phys. Rev. Lett.* **125**, 058103 (2020).
- [96] F. Ferretti, V. Chardès, T. Mora, A. M. Walczak, and I. Giardina, *Phys. Rev. X* **10**, 031018 (2020).
- [97] D. Hartich and U. Seifert, *Phys. Rev. E* **94**, 042416 (2016).
- [98] A. Dembo and O. Zeitouni, *Large Deviations Techniques and Applications* (Springer Berlin Heidelberg, 2010).
- [99] A. Meurer, C. P. Smith, M. Paprocki, O. Čertík, S. B. Kirpichev, M. Rocklin, A. Kumar, S. Ivanov, J. K. Moore, S. Singh, T. Rathnayake, S. Vig, B. E. Granger, R. P. Muller, F. Bonazzi, H. Gupta, S. Vats, F. Johansson, F. Pedregosa, M. J. Curry, A. R. Terrel, v. Roučka, A. Saboo, I. Fernando, S. Kulal, R. Cimrman, and A. Scopatz, *PeerJ Comput. Sci.* **3**, e103 (2017).
- [100] C. Dieball and A. Godec, *Feynman-Kac theory of time-integrated functionals: Itô versus functional calculus* (2022), arXiv:2206.04034 [cond-mat.stat-mech].

**Supplementary Material for:  
Mathematical, Thermodynamical, and Experimental Necessity for Coarse Graining Empirical  
Densities and Currents in Continuous Space**

Cai Dieball and Aljaž Godec

*Mathematical bioPhysics Group, Max Planck Institute for Multidisciplinary Sciences, Am Fassberg 11, 37077  
Göttingen*

In this Supplementary Material (SM) we present an explicit numerical confirmation that a discretely observed diffusion is *not* a Markov process. Moreover, we apply the results for the limit of small window sizes to current fluctuations in a Markov jump process in discretized space. Finally, we list the information that is necessary to reproduce all simulations and analytical results shown in the figures presented the Letter. Further details and derivations related to statements in the Letter can be found in accompanying extended manuscript [1].

**CONTENTS**

I.	Quantification of non-Markovianity of diffusion observed in discrete space (i.e. on a grid)	1
II.	Implications for fluctuations in Markov jump processes on a grid	2
III.	Numerical and analytical evaluation used for the figures	4
	A. Analytical results for the two-dimensional Ornstein-Uhlenbeck process	4
	B. Details and simulation parameters for figures in the Letter	5
	References	6

**I. QUANTIFICATION OF NON-MARKOVIANITY OF DIFFUSION OBSERVED IN DISCRETE SPACE  
(I.E. ON A GRID)**

In this section we provide a quantitative example for the statement made in the Letter that "a continuous dynamics observed on a discrete space is *not* Markovian". This in particular demonstrates that a Markov-jump description with a limited number of states in general *cannot* accurately describe a diffusion process in continuous space. A Markov-jump description may be accurate in systems with a time-scale separation (e.g. as a result of high energy barriers separating minima) on time scales sufficiently larger than the slowest relaxation (e.g. much larger than the longest relaxation time in the minima). However, in general an accurate Markov-jump representation requires too many states to describe diffusive dynamics, and in particular to accurately describe functionals of paths [2]. The example we provide here is the Ornstein-Uhlenbeck process with a rotational flow, see Fig. 1c in the Letter. To quantify the non-Markovianity we discretize the dynamics on a finite grid and quantify violations of the Chapman-Kolmogorov equation, as described in Ref. [3].

We consider the Ornstein-Uhlenbeck process in two-dimensional continuous space, i.e. Eq. (S10) with  $r = D = 1$  and  $\Omega = 3$ . Then we divide the area  $[-5, 5] \times [-5, 5]$  into  $N \times N$  squares  $S_i$  that we label by an index  $i \in \{1, \dots, N^2\}$ . We define the steady-state occupation of the state  $i$  (i.e. of the area/square  $S_i$ ) from the continuous-space steady-state density  $p_s(\mathbf{x}_0)$  (see Eq. (S12)) as

$$p_s(i_0) \equiv \int_{x_0 \in S_{i_0}} d^2 x_0 p_s(\mathbf{x}_0), \quad (\text{S1})$$

and, for any time  $t$ , from the continuous-space propagator (i.e. conditional density)  $G(\mathbf{x}, t | \mathbf{x}_0)$  (see Eq. (S13)) we define the propagator of the discrete space observation as

$$G(i, t | i_0) \equiv \frac{1}{p_s(i_0)} \int_{x \in S_i} d^2 x \int_{x_0 \in S_{i_0}} d^2 x_0 G(\mathbf{x}, t | \mathbf{x}_0) p_s(\mathbf{x}_0). \quad (\text{S2})$$

Moreover, we define [3]

$$G_{t'}^{\text{CK}}(i, t|i_0) \equiv \sum_{j=1}^{N^2} G(i, t-t'|j)G(j, t'|i_0). \quad (\text{S3})$$

Note that by the Chapman-Kolmogorov equation a Markov process would obey  $G_{t'}^{\text{CK}}(i, t|i_0) = G(i, t|i_0)$  for all  $i, i_0, t, t'$ . To quantify non-Markovianity we compute the Kullback-Leibler divergence between  $G$  and  $G^{\text{CK}}$ ,

$$\mathcal{D}_{\text{KL}}^{\text{CK}}(t', t, i_0) \equiv \sum_{i=1}^{N^2} G(i, t|i_0) \ln \left[ \frac{G(i, t|i_0)}{G_{t'}^{\text{CK}}(i, t|i_0)} \right]. \quad (\text{S4})$$

The results for this example are shown in Fig. S1a. Whenever  $\mathcal{D}_{\text{KL}}^{\text{CK}} > 0$  the process is non-Markovian. However, the exact value of  $\mathcal{D}_{\text{KL}}^{\text{CK}} \neq 0$  does not have a direct interpretation. To gain some intuition about the actual value, in Fig. S1b we normalize by the Kullback-Leibler divergence of  $G$  and  $p_s$ ,

$$\mathcal{D}_{\text{KL}}^{\text{ps}}(t, i_0) \equiv \sum_{i=1}^{N^2} G(i, t|i_0) \ln \left[ \frac{G(i, t|i_0)}{p_s(i)} \right]. \quad (\text{S5})$$

The rationale is that the actual value (at least) should not directly depend on how far the actual dynamics is displaced from the steady state, i.e. if the dynamics is closer to the steady state the same value of  $\mathcal{D}_{\text{KL}}^{\text{CK}}$  should be interpreted as stronger violation of Markovianity as compared to when it is farther away, since the actual dynamics changes less in magnitude in the former case.

As expected, the extent of the violation of Markovianity depends on the grid-size. It reduces for sufficiently small grids (large  $N$ ), i.e. the dynamics become effectively Markovian on shorter time-scales, as well as for large “ignorant” discrete observations (small  $N$ ), where all probability flows are averaged over. Both limits are intuitive—non-Markovianity arises because there is no time-scale separation ensuring local-equilibrium. That is, the direction and rate of leaving a discretely observed state depends on the previous state and the precise location of entering the binned discrete state. Notably (and obviously), the dynamics in the limit of infinite number of grid points, i.e. in the continuum limit, is exactly the diffusion process and thus Markovian. Moreover, the attenuation of non-Markovianity for very “ignorant” grids (i.e. small number of states) as a result of spatial averaging over large regions is easiest understood by realizing that the dynamics with one state is (trivially) Markovian and stationary at all times, the dynamics with two states slightly less so, etc.

**A diffusion observed on a grid is thus *not* a Markov jump process** and one in general requires many states for an accurate discrete-state Markov-jump representation, which is typically not experimentally feasible. Moreover, one actually needs to parameterize the Markov state model with such a large number of states, which is even less feasible. **In contrast, evaluating empirical densities and currents in finite windows assuming an underlying continuous-space diffusion—as carried out in the present work—is *not* constrained to small windows *nor* does it require any parameterization of a discrete-state model for its interpretation.**

## II. IMPLICATIONS FOR FLUCTUATIONS IN MARKOV JUMP PROCESSES ON A GRID

If one approximates  $d \geq 2$ -dimensional continuous-space dynamics by a Markov jump process on a grid, the fact that the Markov-jump description becomes asymptotically accurate for the number of states  $N \rightarrow \infty$  implies that for large  $N$ , correlations and fluctuations of densities and currents will be governed by the limits for  $h \rightarrow 0$  in Eq. (6) in the Letter. Corresponding to the problems with large deviation theory for  $h \rightarrow 0$  discussed in the appendix, central-limit large deviations in dimensions  $d \geq 2$  exist only for finite grids (corresponding to  $h > 0$ ). In contrast, in the continuum limit where the number of states tends to infinity (see e.g. [5]; corresponding to  $h \rightarrow 0$ ) the recurrence time to visit a state diverges, which would require  $t > \infty$  for validity of the large deviation principle. In particular, a finite relaxation time scale (where the relaxation time is the inverse of the smallest non-zero eigenvalue of the generator of the dynamics) that remains finite in the continuum limit alone does not guarantee the validity of the large deviation principle.

We now give a specific example for the validity of the limits for  $h \rightarrow 0$  in Eq. (6) in the Letter. A state at position  $\mathbf{x}$  of a Markov jump process on a grid with spacing  $h$  can asymptotically be interpreted as corresponding to a window function  $U_{\mathbf{x}}^h$  that is the normalized indicator function of a square with spacing  $h$  around  $\mathbf{x}$ , e.g. in two-dimensional space  $U_{\mathbf{x}}^h(x', y') = h^{-2} \mathbb{1}_{|x-x'|, |y-y'| \leq h/2}$ . With this correspondence, applied to a two-dimensional

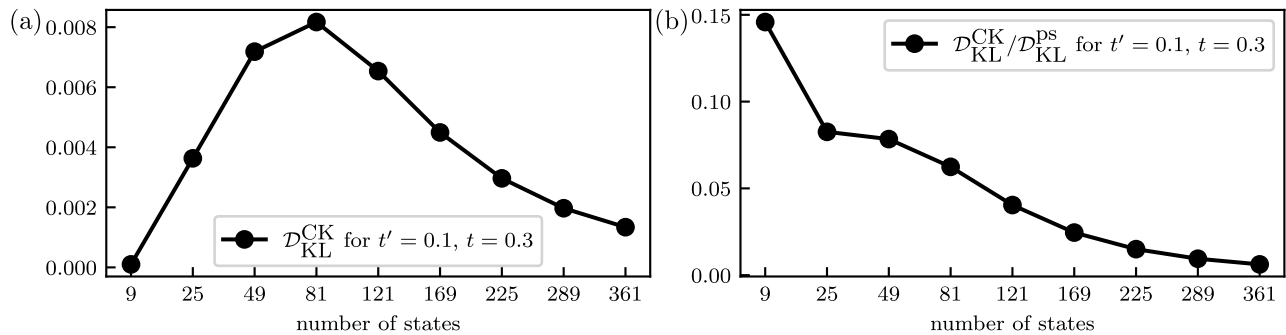


FIG. S1. Quantification of non-Markovianity (as described in the text) in a discrete-space observation with  $N \times N$  states for  $N = 3, 5, 7, \dots, 19$ . The integrals in Eq. (S2) were evaluated numerically. (a) The value of  $\mathcal{D}_{\text{KL}}^{\text{CK}}(t', t, i_0)$ , for  $i_0$  denoting the index of the square containing the point  $(0, 0)$ , obviously decreases for large numbers of states according to expectations. For very small numbers of states, where very few details of the dynamics are observed, the non-Markovianity also appears to be smaller. (b) To gain intuition about the values of  $\mathcal{D}_{\text{KL}}^{\text{CK}}(t', t, i_0)$  we normalized it by  $\mathcal{D}_{\text{KL}}^{\text{PS}}(t, i_0)$ , i.e. a value of 1 means that the Kullback-Leibler divergence of  $G$  and  $G^{\text{CK}}$  equals the divergence of  $G$  and  $G^{\text{PS}}$ . Since the Kullback-Leibler divergence is *not* a metric (it is not symmetric and does not satisfy the triangle inequality), one should be careful when interpreting its values *quantitatively*.

example with constant isotropic diffusion, the current fluctuations for a small grid-spacing  $h$  should according to Eq. (6) in the Letter (see accompanying paper for prefactor  $2D$ ) be governed by

$$\text{var}_{\mathbf{J}}^{\mathbf{x}}(t) \stackrel{h \rightarrow 0}{\approx} \frac{2D}{t} p_{\mathbf{s}}(\mathbf{x})(d-1)h^{-2} + \mathcal{O}(t^{-1})\mathcal{O}(h^{-1}). \quad (\text{S6})$$

Rates  $k_{i \rightarrow i'}^{j \rightarrow j'}$  (denoting  $x$ -indices by  $i$  and  $y$ -indices by  $j$ ) for a discretized process originating from continuous dynamics are not unique, but can e.g. be obtained following [4]. Via the pseudo potentials (we need to use *pseudo* potentials since we consider a non-equilibrium process [4])

$$\begin{aligned} \tilde{U}(x, y) &= \frac{r}{2D}x^2 - \frac{\Omega}{D}xy \\ \tilde{V}(x, y) &= \frac{r}{2D}y^2 + \frac{\Omega}{D}xy, \end{aligned} \quad (\text{S7})$$

we obtain rates

$$\begin{aligned} k_{i \rightarrow i \pm 1}^{j \rightarrow j} &= \frac{D}{h^2} \exp\left(-\frac{1}{2}[\tilde{U}(x_{i \pm 1}, y_j) - \tilde{U}(x_i, y_j)]\right) \\ k_{i \rightarrow i}^{j \rightarrow j \pm 1} &= \frac{D}{h^2} \exp\left(-\frac{1}{2}[\tilde{V}(x_i, y_{j \pm 1}) - \tilde{V}(x_i, y_j)]\right). \end{aligned} \quad (\text{S8})$$

Note that all other rates (i.e. to non-neighboring states) vanish in this construction.

Currents are now defined as transition counts on the edges of the grid. To compare to continuous-space time-averaged currents, we define the  $x$ -component of a current  $\bar{\mathbf{J}}_{\mathbf{x}}$  at a grid point  $\mathbf{x}$  as the net number of transitions on the edge to the right of  $\mathbf{x}$  and the  $y$ -component as the net number of transitions on the edge above  $\mathbf{x}$ . Note that this current reflects probabilities of transitions and not probability densities which differs by the current density by a factor of  $h^2$ , i.e. by the area corresponding to of a state. With this definition, the limit Eq. (S6) for  $h \rightarrow 0$  becomes

$$\text{var}_{\mathbf{J}}^{\mathbf{x}}(t) \stackrel{h \rightarrow 0}{\approx} \frac{2D}{t} p_{\mathbf{s}}(\mathbf{x})(d-1) + \mathcal{O}(t^{-1})\mathcal{O}(h^1). \quad (\text{S9})$$

Note that one could instead equivalently define the current with the normalization  $h^{-2}$  to obtain densities and use the limit in Eq. (S6).

Fig. S2 illustrates the validity of the limit Eq. (S9) for a discretized Ornstein-Uhlenbeck process, see Eq. (S10) with  $r = D = 1, \Omega = 3$ . The process on the area  $[-5, 5]^2$  is discretized into a  $101 \times 101 = 10201$ -state Markov jump process, i.e. the grid spacing is  $h = 0.1$ . The quantitative agreement of Fig. S2c and d illustrates that the limit current fluctuations on the jump process are indeed governed by Eq. (S9). Note that the  $t^{-1}$  scaling of the  $h^{-2}$  term in Eq. (S9) ensures that for  $h \rightarrow 0$  current fluctuations are governed by this equation for all time-scales.

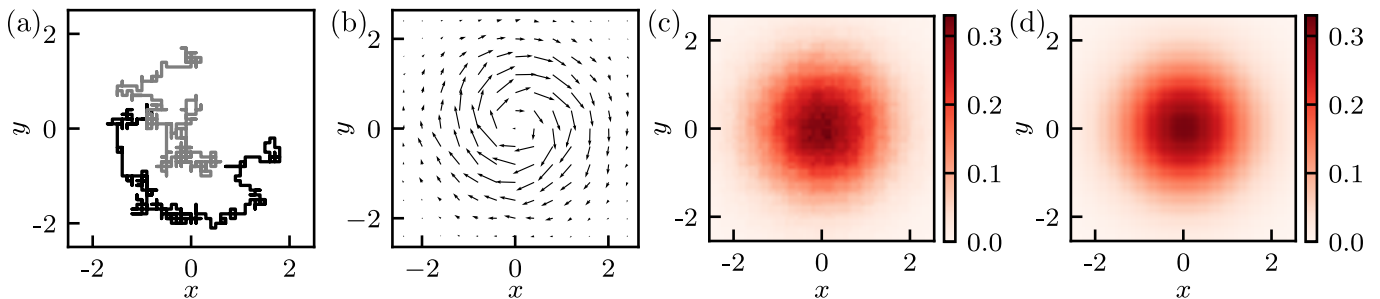


FIG. S2. (a) Two sample trajectories of the Ornstein-Uhlenbeck process discretized as described in the text with time step  $dt = 0.001$  and total time  $T = 1$ , starting in steady-state initial conditions. (b) Mean current as defined in the text obtained from a simulation of 10,000 trajectories such as the ones in (a). For visibility arrows are only drawn at every fourth  $x$  and  $y$  value contained in the grid. (c) Variance of the current at individual grid points obtained from the same simulation as in (b). (d) Eq. (S9) evaluated at individual grid points. The qualitative and quantitative agreement with (c) shows that Eq. (S9), which was derived in continuous space, has direct consequences for Markov jump processes on grids with small  $h$ .

### III. NUMERICAL AND ANALYTICAL EVALUATION USED FOR THE FIGURES

This section gives further parameters and all details necessary to reproduce all figures in the Letter.

#### A. Analytical results for the two-dimensional Ornstein-Uhlenbeck process

For the numerical and analytical results shown in Figs. 1 and 3 in the Letter, we use the two-dimensional Ornstein-Uhlenbeck process given by the Langevin equation

$$d\mathbf{x}_t = \mathbf{F}_{\text{rot}}(\mathbf{x}_t)dt + \sqrt{2D}d\mathbf{W}_t, \quad (\text{S10})$$

with drift field  $\mathbf{F}_{\text{rot}}(\mathbf{x}) = -\Theta\mathbf{x}$  where  $\Theta = \begin{bmatrix} r & -\Omega \\ \Omega & r \end{bmatrix}$ ,  $r > 0$ . The drift part splits into

$$\mathbf{F}_{\text{rot}}(\mathbf{x}) = -D\{\nabla\phi(\mathbf{x})\} + \mathbf{j}_s(\mathbf{x})/p_s(\mathbf{x}), \quad (\text{S11})$$

with potential  $\phi(\mathbf{x}) = \frac{r}{2D}\mathbf{x}^T\mathbf{x}$  and steady-state density and current

$$p_s(\mathbf{x}) = \frac{r}{2\pi D}e^{-r\frac{\mathbf{x}^T\mathbf{x}}{2D}}$$

$$\mathbf{j}_s(\mathbf{x}) = (\mathbf{F} - D\nabla_{\mathbf{x}})p_s(\mathbf{x}) = \Omega p_s(\mathbf{x}) \begin{bmatrix} x_2 \\ -x_1 \end{bmatrix}. \quad (\text{S12})$$

A straightforward left-right decomposition [6] gives the propagator/two-point function

$$G(\mathbf{x}, t'|\mathbf{x}_0) = \frac{r}{2\pi D(1 - e^{-2rt'})} \exp \left[ \frac{-r \left( \mathbf{x} - e^{-rt'} \begin{bmatrix} \cos(\Omega t') & \sin(\Omega t') \\ -\sin(\Omega t') & \cos(\Omega t') \end{bmatrix} \mathbf{x}_0 \right)^2}{2D(1 - e^{-2rt'})} \right]$$

$$P_{\mathbf{x}_0}(\mathbf{x}, t') \equiv G(\mathbf{x}, t'|\mathbf{x}_0)p_s(\mathbf{x}_0). \quad (\text{S13})$$

We then analytically solve the necessary Gaussian integrals for Gaussian window functions

$$U_{\mathbf{x}}^h(\mathbf{z}) = (2\pi h^2)^{-d/2} \exp \left[ -\frac{(\mathbf{z} - \mathbf{x})^2}{2h^2} \right], \quad (\text{S14})$$

and numerically solve the remaining  $t'$ -integral. This enables a very fast and stable (even for very small coarse graining where numerical spatial integrals would eventually fail) computation of the second moments shown in Figures 2 and 3. The analytical integrals were performed with the Python-based computer algebra system SymPy [7]. To give an

example, we now show the computation of one of the terms in the current variance result in Eq. (5) in the Letter (other terms similarly).

We start e.g. with the spatial integrals

$$\int d^2x \int d^2x_0 V(\mathbf{x}) U(\mathbf{x}_0) j_s^2(\mathbf{x}) j_s^2(\mathbf{x}_0) G(\mathbf{x}, t | \mathbf{x}_0) p_s(\mathbf{x}_0), \quad (\text{S15})$$

where we set  $\mathbf{x} = (x_1, x_2)$ ,  $\mathbf{x}_0 = (x_3, x_4)$  such that  $j_s^2(\mathbf{x}) = -\Omega x_1$  and  $j_s^2(\mathbf{x}_0) = -\Omega x_3$  and we use constants  $\{c_i\}$  to write

$$\begin{aligned} V(\mathbf{x}) &= \frac{c_1}{\pi} e^{-c_1((x_1-y_1)^2+(x_2-y_2)^2)} \\ U(\mathbf{x}_0) &= \frac{c_2}{\pi} e^{-c_2((x_3-y_3)^2+(x_4-y_4)^2)} \\ p_s(\mathbf{x}_0) &= \frac{c_3}{\pi} e^{-c_3(x_3^2+x_4^2)} \\ G(\mathbf{x}, t | \mathbf{x}_0) &= \frac{c_4}{\pi} e^{-c_4((c_5x_3+c_6x_4-x_1)^2+(c_5x_4-c_6x_3-x_2)^2)}. \end{aligned} \quad (\text{S16})$$

Integrating from  $-\infty$  to  $\infty$  over  $x_3$  and  $x_4$  gives (Gaussian integrals with  $c_1, c_2, c_3, c_4 > 0$ )

$$\begin{aligned} \int d^2x_0 V(\mathbf{x}) U(\mathbf{x}_0) j_s^2(\mathbf{x}) j_s^2(\mathbf{x}_0) G(\mathbf{x}, t | \mathbf{x}_0) p_s(\mathbf{x}_0) &= \frac{\Omega^2 c_1 c_2 c_3 c_4 x_1 (c_2 y_3 + c_4 c_5 x_1 - c_4 c_6 x_2)}{\pi^3 (c_2 + c_3 + c_4 c_5^2 + c_4 c_6^2)^2} \times \\ &e^{\frac{c_2^2 y_4^2 + 2c_2 c_4 y_4 (c_5 x_2 y_4 + c_6 x_1) + c_4^2 (c_5 x_2 + c_6 x_1)^2 + (c_2 y_3 + c_4 c_5 x_1 - c_4 c_6 x_2)^2}{c_2 + c_3 + c_4 c_5^2 + c_4 c_6^2} - c_1 x_1^2 + 2c_1 x_1 y_1 - c_1 x_2^2 + 2c_1 x_2 y_2 - c_1 (y_1^2 + y_2^2) - c_2 (y_3^2 + y_4^2) - c_4 (x_1^2 + x_2^2)}. \end{aligned} \quad (\text{S17})$$

To integrate over  $x_1$  and  $x_2$ , we simply use ( $a_4, a_5 > 0$ )

$$\begin{aligned} \int_{-\infty}^{\infty} dx_1 \int_{-\infty}^{\infty} dx_2 (a_1 x_1 + a_2 x_1^2 + a_3 x_1 x_2) e^{-a_4 x_1^2 - a_5 x_2^2 + a_6 x_1 + a_7 x_2 + a_8} \\ = \frac{\pi (2a_1 a_4 a_5 a_6 + a_2 a_5 (2a_4 + a_6^2) + a_3 a_4 a_6 a_7) e^{\frac{4a_5 a_8 + a_7^2}{4a_5} + \frac{a_6^2}{4a_4}}}{4a_4^{\frac{5}{2}} a_5^{\frac{3}{2}}}. \end{aligned} \quad (\text{S18})$$

Equations for the  $\{a_i\}$  in terms of the  $\{c_i\}$  can be read off Eq. (S17) and the  $\{c_i\}$  contain all parameter dependencies of the process, including the  $t'$ . The  $t'$ -integration is then performed numerically.

## B. Details and simulation parameters for figures in the Letter

The process in Fig. 1a,b in the Letter is simulated as a free two-dimensional Brownian motion. Numerical Stratonovich integration gives the empirical density and current. The times shown are  $\tau_1^- = 1.14$ ,  $\tau_1^+ = 3.83$ ,  $\tau_2^- = 6.54$ ,  $\tau_2^+ = 6.80$ .

The mean and variance in the histograms in Fig. 1d,e and the relative error in Fig. 1f in the Letter are obtained analytically as described above. The TUR-bound is given by  $\frac{2}{\sigma t}$  where  $\sigma = \frac{2\Omega^2}{r}$  is the dissipation in the steady state of the Ornstein-Uhlenbeck process (S10) (see [1]). For  $\Omega = 5, r = 1, t = 5$  we obtain that the TUR-bound shown in Fig. 1f in the Letter the is at 0.008.

The process in Fig. 2 in the Letter is the shear flow with  $\mathbf{F}(x, y) = 2x\hat{\mathbf{y}}$  and  $\mathbf{D} = \mathbf{1}$  from  $(0, 0)$  to  $(2, 0)$  in total time  $t_2 - t_1 = 1$ . It is simulated with time step size  $dt = 0.02$  as Brownian bridge in  $x$ -direction (exactly hits 2 after time 1) and then pick trajectories that hit  $y_{\text{final}} = 0$  with deviation less than 0.02. Time-reversed and dual reversed trajectories are similarly from  $(2, 0)$  to  $(0, 0)$  with same or inverted shear. For each transition around 11,000 – 12,000 trajectories were considered. Arrows are in direction of the first/last step in discretized time.

The trajectory in Fig. 2e in the Letter is sampled from an Ornstein-Uhlenbeck process Eq. (S10) with  $\Omega = 3, r = D = 1$  and total time  $t \approx 37$ .

The simulations in Fig. 3 in the Letter are performed with time step  $dt = 10^{-4}$  and 8192 repetitions for 3a and 4096 repetitions for 3b. All simulations are performed by discretizing Eq. (S10) and sampling the initial point  $\mathbf{x}_0$

from the steady-state distribution  $p_s(\mathbf{x})$ . Additional parameters in 3c are  $h = 1, 0.25, 0.03$  from dark to bright.

- 
- [1] C. Dieball and A. Godec, (2022), [arXiv:2204.06553 \[cond-mat.stat-mech\]](#).
  - [2] E. Suárez, R. P. Wiewiora, C. Wehmeyer, F. Noé, J. D. Chodera, and D. M. Zuckerman, *J. Chem. Theory Comput.* **17**, 3119 (2021).
  - [3] A. Lapolla and A. Godec, *Phys. Rev. Research* **3**, L022018 (2021).
  - [4] V. Holubec, K. Kroy, and S. Steffenoni, *Phys. Rev. E* **99**, 032117 (2019).
  - [5] T. R. Gingrich, G. M. Rotskoff, and J. M. Horowitz, *J. Phys. A: Math. Theor.* **50**, 184004 (2017).
  - [6] C. W. Gardiner, *Handbook of stochastic methods for physics, chemistry, and the natural sciences* (Springer-Verlag, Berlin New York, 1985).
  - [7] A. Meurer, C. P. Smith, M. Paprocki, O. Čertík, S. B. Kirpichev, M. Rocklin, A. Kumar, S. Ivanov, J. K. Moore, S. Singh, T. Rathnayake, S. Vig, B. E. Granger, R. P. Muller, F. Bonazzi, H. Gupta, S. Vats, F. Johansson, F. Pedregosa, M. J. Curry, A. R. Terrel, v. Roučka, A. Saboo, I. Fernando, S. Kulal, R. Cimrman, and A. Scopatz, *PeerJ Comput. Sci.* **3**, e103 (2017).